

Generalized-Ensemble Simulations of the Human Parathyroid Hormone Fragment PTH(1-34)

Ulrich H.E. Hansmann *

Department of Physics, Michigan Technological University, Houghton, MI 49931-1295, USA

(Dated: October 5, 2018)

Abstract

A generalized-ensemble technique, multicanonical sampling, is used to study the folding of a 34-residue human parathyroid hormone fragment. An all-atom model of the peptide is employed and the protein-solvent interactions are approximated by an implicit solvent. Our results demonstrate that generalized-ensemble simulations are well suited to sample low-energy structures of such large polypeptides. Configurations with a root-mean-square deviation (rmsd) to the crystal structure of less than one Å are found. Finally, we discuss limitations of our implicit solvent model.

* ph.: 906-487-2909; fax: 906-487-2933; hansmann@mtu.edu

I. INTRODUCTION

The successful deciphering of the human genome has aggravated an old challenge in protein science: for most of the resolved protein sequences we do not know the corresponding structures and functions. Computer experiments offer one way to evaluate the sequence-structure relationship but are extremely difficult for realistic protein models where interactions among all atoms are taken into account. The complex form of the intramolecular forces and of the interaction with the solvent, containing both repulsive and attractive terms, leads to a very rough energy landscape with a huge number of local minima. These minima are separated by energy barriers that are much higher than the typical thermal energy of a protein (of order $k_B T$) at room temperature. Hence, simple canonical Monte Carlo or molecular dynamics simulations will get trapped in a local minimum and often not thermalize within a finite amount of available CPU time. While this multiple minima problem does not necessarily inhibit molecular dynamics or Monte Carlo studies of peptides and proteins^{1,2}, it restricts calculation of accurate *thermodynamic* averages to small peptides³.

A number of novel simulation techniques have been proposed for overcoming this multiple-minima problem (for a review, see Ref. 4). Important recent examples can be found in Ref. 5,6. Another example is parallel tempering, also known as replica exchange method and introduced to protein science in Ref. 7, that has become increasingly popular over the last few years^{8,9,10}. Parallel tempering is only one example of a class of new and sophisticated algorithms commonly summarized as *generalized-ensemble* methods¹¹. In this article, we are concerned with another generalized-ensemble technique, multicanonical sampling¹², that was first applied to the protein-folding problem in Ref. 13. Its usefulness for calculating reliable thermodynamic quantities at low temperatures has been established for small peptides of up to ≈ 20 residues^{13,14,15}. However, stable domains in proteins consist usually of 40-200 amino acids. Hence, it is necessary to evaluate the effectiveness of this approach for larger molecules than the peptides investigated so far. For this purpose, we have performed generalized-ensemble simulations of the peptide fragment PTH(1-34) corresponding to residues 1-34 of human parathyroid hormone^{16,17,18}.

The 84-amino acid human parathyroid hormone is involved in the regulation of the calcium level in blood and influences bone formation¹⁹. The NH₂-terminal 34 residues of the hormone, further on referred to as PTH(1-34), are sufficient for the biological activities of this

hormone suggesting medical and pharmaceutical applications of the peptide²⁰. The crystal structure of the peptide has been resolved at 0.9 Å and resembles a slightly bend long helix (PDB code 1ET1)¹⁷. NMR studies of the peptide in solution under near physiological conditions (PDB code 1ZWA)¹⁸ and in 20 % trifluoroethanol solution (PDB code 1HPY)¹⁸ rather indicate an ensemble of structures that have in common two helices separated by a disordered region.

In the present article, we try to overcome the problems of previous simulated annealing simulations of PTH(1-34)²¹, that did not allow a detailed structure evaluation, by using multicanonical sampling¹², one of the most prominent generalized-ensemble techniques. An all-atom representation of the molecule is employed and the intramolecular interactions are described by the ECEPP/3 force field²². The protein-solvent interactions are approximated by the solvent accessible surface term of Ooi *et al.*²³ Quantities such as the average helicity, number of contacts, average energy, and specific heat are calculated. Our results demonstrate the feasibility of generalized-ensemble simulations for large molecules such as PTH(1-34). In addition, they indicate that with the advent of these and other modern search techniques, structure prediction of proteins is limited more by current energy functions (and especially solvent approximations) than by the simulation algorithms.

II. METHODS

Our research into the thermodynamics of PTH(1-34) is based on a detailed, all-atom representation of that peptide. The interactions between the atoms are described by a standard force field, ECEPP/3²² (as implemented in the program package SMMP²⁴), and are given by the sum of the electrostatic term E_C , the Lennard-Jones energy E_{LJ} , hydrogen-bond term E_{HB} for all pairs of atoms in the peptide together with the torsion term E_{tor} for all torsion angles:

$$E_{ECEPP/2} = E_C + E_{LJ} + E_{HB} + E_{tor}, \quad (1)$$

$$E_C = \sum_{(i,j)} \frac{332q_i q_j}{\epsilon r_{ij}}, \quad (2)$$

$$E_{LJ} = \sum_{(i,j)} \left(\frac{A_{ij}}{r_{ij}^{12}} - \frac{B_{ij}}{r_{ij}^6} \right), \quad (3)$$

$$E_{HB} = \sum_{(i,j)} \left(\frac{C_{ij}}{r_{ij}^{12}} - \frac{D_{ij}}{r_{ij}^{10}} \right), \quad (4)$$

$$E_{tor} = \sum_l U_l (1 \pm \cos(n_l \chi_l)). \quad (5)$$

Here, r_{ij} (in Å) is the distance between the atoms i and j , χ_l is the torsion angle for the chemical bond l and n_l characterizes its symmetry. The charges and force field parameters $q_i, A_{ij}, B_{ij}, C_{ij}, D_{ij}, U_l$ were calculated from crystal structures of amino acids using semi-empirical methods. The dielectricity constant is set to $\epsilon = 2$, its common value in ECEPP calculations. Since the bond lengths are fixed in ECEPP, the backbone torsion angles ϕ, ψ, ω and the side chain torsion angles χ are the true degrees of freedom. Hence, in a Monte Carlo (MC) sweep single angles are updated sequentially by the Metropolis algorithm. The protein-water interactions are approximated by a solvent-accessible surface term

$$E_{solv} = \sum_i \sigma_i A_i, \quad (6)$$

where A_i is the solvent accessible surface area of the i -th atom in the present configuration, and σ_i the solvation parameter for the atom i . We choose the solvation parameter set OONS of Ref.²³ that is often used together with the ECEPP force field. The potential energy of the solvated molecule is then given by

$$E_{tot} = E_{ECEPP/3} + E_{solv} \quad (7)$$

In such a detailed protein model, the various competing interactions lead model to an energy landscape with a multitude of local minima separated by high-energy barriers. Canonical Monte Carlo or molecular dynamics simulations will likely get trapped in one of these minima and not thermalize within the available CPU time. Only recently, with the introduction of new and sophisticated algorithms such as *generalized-ensemble* techniques¹¹ was it possible to alleviate this problem in protein simulations¹³. For simulating PTH(1-34) we have chosen one most commonly used generalized-ensemble technique, multicanonical sampling¹².

The multicanonical algorithm¹² assigns a weight $w_{mu}(E) \propto 1/n(E)$ to conformations with energy E . Here, $n(E)$ is the density of states. A simulation with this weight leads to a uniform distribution of energy:

$$P_{mu}(E) \propto n(E) w_{mu}(E) = \text{const}. \quad (8)$$

Thus, the simulation generates a 1D random walk in the energy space, allowing itself to escape from any local minimum. Since a large range of energies is sampled, re-weighting²⁵ allows one to calculate thermodynamic quantities over a wide range of temperatures T by

$$\langle \mathcal{A} \rangle_T = \frac{\int dx \mathcal{A}(x) w^{-1}(E(x)) e^{-\beta E(x)}}{\int dx w^{-1}(E(x)) e^{-\beta E(x)}}, \quad (9)$$

where x stands for configurations, $E(x)$ for its total potential energy $E(x) = E_{ECEPP/3}(x) + E_{solv}(x)$ and β for the inverse temperature, $\beta = 1/k_B T$.

Unlike in constant temperature simulations the weights are not *a priori* known in multicanonical simulations. In fact, knowledge of the exact weights is equivalent to obtaining the density of states $n(E)$, i.e., solving the system. However, for a numerical simulations estimators are sufficient as long as these do not deviate not too much from $n^{-1}(E)$. This is because the same weights that are used for the simulation appear also in the re-weighting procedure of Eq. 9. In the present study, we calculate these estimators from a preliminary simulated annealing run of 80,000 MC-sweeps using the method described in Ref. 26. All thermodynamic quantities are then estimated from one production run of 1,000,000 sweeps, starting from a random initial configuration and after discarding 10,000 sweeps for thermalization. We store in every fifth sweep for further analysis various physical quantities and the dihedral angles of the current configuration. Our error bars are estimated by dividing this time series of data into 8 bins of each 125,000 sweeps.

III. RESULTS AND DISCUSSION

We start our analysis by calculating thermodynamic averages of the intramolecular energy $\langle E_{ECEPP/3} \rangle (T)$ and the solvation energy $\langle E_{SOLV} \rangle (T)$. Both quantities and the resulting total energy $\langle E_{TOT} \rangle (T) = \langle E_{ECEPP/3} + E_{SOLV} \rangle (T)$ are displayed as function of temperature in Fig. 1. The thermal behavior of the peptide is characterized by a competition between intramolecular and solvation energy. While $\langle E_{ECEPP/3} \rangle (T)$ decreases with decreasing temperature, $\langle E_{SOLV} \rangle (T)$ increases toward lower temperatures. The interplay of both terms leads to two temperature regimes that are separated by a steep decrease in the total energy $\langle E_{TOT} \rangle (T)$. The corresponding pronounced peak in the specific heat per residue

$$C(T) = \beta^2 (\langle E_{TOT}^2 \rangle (T) - \langle E_{TOT} \rangle^2 (T)) / 34, \quad (10)$$

displayed in the inset, marks the transition temperature at $T_c = 560 \pm 10$ K.

The structural changes associated with this transition can be deduced from Fig. 2 where we display the average helicity $\langle n_H \rangle (T)$ as a function of temperature. Here, we have defined n_H as the number of residues whose pair of backbone dihedral angles (ϕ, ψ) takes values in the range: $(-70^\circ \pm 30^\circ, -37^\circ \pm 30^\circ)$. We see from the plot of both quantities that the high-temperature (high-energy) region is characterized by configurations with vanishing helicity ($\approx 10\%$) while at low temperatures (and, correspondingly, low energies) configurations dominate that are almost completely helical ($\approx 90\%$ of the residues are part of a helix). The pronounced peak at T_c in the susceptibility (per residue)

$$\chi(T) = (\langle n_H^2 \rangle - \langle n_H \rangle^2) / 34, \quad (11)$$

shown in the inset, is further proof for the sharp transition between low-energy helical states and high-energy disordered coil states. Associated with this helix-coil transition is also a decrease in the solvent accessible volume $\langle V \rangle (T)$ as calculated by the double cubic lattice method²⁷ (data not shown). Above T_c , the average volume is $\langle V \rangle \approx 10000 \text{ \AA}^3$, while below T_c the volume is reduced to $\langle V \rangle \approx 9000 \text{ \AA}^3$.

The modest decrease in $\langle V \rangle$ together with the large value of the helicity $\langle n_H \rangle (T)$ indicate that below T_c a single elongated helix is the dominant structure for PTH(1-34). Indeed, we find in our simulation as lowest-energy state an elongated helix with 31 residues part of the helix. This structure, shown in Fig. 3b, has not only the lowest *total* energy ($E_{TOT} = -277.8$ kcal/mol), but also the lowest *intramolecular* energy: $E_{ECEPP/3} = -136.5$ kcal/mol. It is very similar to the crystal structure of PTH(1-34) (PDB code 1ET1, displayed in Fig. 3a) where also 31 residues are part of an α -helix and whose energy after regularization with the program FANTOM²⁸ is $E_{TOT} = -277.9$ kcal/mol ($E_{ECEPP/3} = -187.0$ kcal/mol). While our numerically determined structure has a slightly larger solvent-accessible surface area ($A = 3860 \text{ \AA}^2$) than the crystal structure ($A = 3410 \text{ \AA}^2$), it has 95% of all native contacts formed, i.e. 95 % of the contacts between residues found in the crystal structure exist also in our lowest-energy configuration. Here, we consider two residues in contact if the distance between their C_α -atoms is less than 8 \AA , and the two residues are neither neighbor nor next-nearest neighbor in the peptide chain. Given that almost all native contacts are formed in the lowest-energy structure, it is not surprising that the root-mean-square deviation (rmsd) between the two structures is only 0.8 \AA for backbone atoms (2.3

Å when all heavy atoms are taken into account). For comparison, the crystal structure of PTH(1-34) (1ET1) itself was solved at 0.9 Å resolution¹⁷. We remark that recent structure determinations of the similar sized villin headpiece subdomain HP-36, a 36-residue peptide, by Energy Landscape Paving²⁹ and parallel tempering⁹ were restricted to an accuracy of ≈ 6 Å. We believe that the higher accuracy of our PTH(1-34) results does not indicate any advantage of multicanonical sampling over the above methods but is rather due to the simpler geometry of PTH(1-34).

At $T = 300$ K, our lowest energy structure appears with a frequency of $(99 \pm 0.5)\%$, i.e. almost all observed configurations resemble the crystal structure. The predominance of this structure is also reflected in the well-developed funnel in Fig. 4 where we display the projection of the free-energy landscape at $T = 300$ K on the number of native contacts. The free energy decreases rapidly with increasing number of native contacts. No indications for competing local minima that could act as traps are observed indicating a rather smooth funnel. On the other hand, at the transition temperature $T_c = 560$ K, the free energy landscape (displayed in the inset) is flat and configurations with small number of native contacts coexist with such that have many native contacts.

However, while the crystal structure is in our simulation the dominant configuration at $T = 300$ K, it differs from the set of NMR-structures found at room temperature. In near-physiological solution, one observes instead two helices separated by a disordered and flexible region. We show in Fig. 3c as an example one of the resolved solution configurations (from 1HPY)¹⁸. The N-terminal helix ranges from Glu₄ to His₉ and the C-terminal helix from Ser₁₇ to Gln₂₉. Addition of trifluoroethanol reduces hydrophobic interactions and increases the length of these helices¹⁸. Hence, our simulation of PTH(1-34) does not reproduce the experimental results for that peptide in solution albeit protein-solvent interactions are considered in our energy function by an approximate term. Instead, our simulation favors the crystal structure of the peptide that is observed in membrane and hydrophobic environments.

In order to understand in greater detail the relation between our simulation results and the NMR experiments, we plot in Fig. 5a for each residue the free energy difference ΔG_i at $T = 300$ K between configurations with residue i part of an α -helix and such where that residue is not part of an α -helix. The free-energy differences are largest for residues Asn₁₆-Lys₂₇, and it is for these residues that first helix formation is observed. A second cluster of

residues that have large free-energy differences are observed between Ile₅ and Asn₁₀. Both regions are separated by residues Leu₁₁ - Leu₁₅ that have smaller free energy differences. The observed free-energy differences are strongly correlated with differences in the (potential) energy ΔE_{TOT} that together with its two components $E_{ECEPP/3}$ and E_{SOLV} are plotted in Fig. 5b. Note, that the variations in the energy differences result from the $E_{ECEPP/3}$ part, i.e. from the intramolecular interactions. The corresponding solvent energies favor in general residues that are not in a helical state but vary little with the residues. In addition, their magnitude is so small that it is difficult to distinguish in the figure between ΔE_{TOT} and $\Delta E_{ECEPP/3}$.

The position of the two helices in the solvent structure of Fig. 3c corresponds to the regions where in our simulation the measured free-energy differences and potential energy differences are large. In the NMR structures, the C-terminal helix is more stable than the N-terminal helix. Similarly, we find larger absolute values of $\Delta G_i \approx -14$ kcal/mol ($\Delta E_{TOT} \approx -39$ kcal/mol) for residues Asn₁₆ to Lys₂₇ (with the maximal values at Arg₂₀: $\Delta G = -19.4$ kcal/mol and $\Delta E_{TOT} = -55.1$ kcal/mol) compared with $\Delta G_i \approx -12$ kcal/mol ($\Delta E_{TOT} \approx -36$ kcal/mol) for residues Ile₅ to Asn₁₀. On the other hand, the flexible region connecting the two helices in the NMR structure corresponds to a region of residues that have with $\Delta G_i \approx -8$ kcal/mol and $\Delta E_{TOT} \approx -25$ kcal/mol considerably smaller free (potential) energy differences. The free-energy differences are smallest for Leu₁₁ and Gly₁₂: $\Delta G_i \approx -6$ kcal/mol and $\Delta E_{TOT} \approx 17$ kcal/mol. The later result is not surprising giving the inherent flexibility of glycine (which, however, is part of the helix in our lowest-energy configuration).

The observed variations in the free and potential energy differences suggest that we may find at higher temperatures configurations similar to the NMR structures. This is because the helix will be de-stabilized with increasing temperature, and more easily for residues Leu₁₁ to Leu₁₅ than in the regions that corresponds to the two terminal helices. In order to test this conjecture, we show in Fig. 6 two quantities as function of temperature. One is the frequency of configurations that have a continuous helix stretching at least between Ile₅ and Lys₂₇ and are therefore similar to the crystal structure of PTH(1-34). The second quantity is the frequency of configurations that have helices stretching at least between Ile₅ and His₉ and between Ser₁₇ and Gln₂₉, but are separated in-between by a non-helical flexible region. Hence, the later quantity measures the frequency of configurations that are similar

to the NMR structure. A typical example of this group of configurations is displayed in Fig. 3d. While this conformation is also a local minimum, its total energy $E_{TOT} = -201.4$ kcal/mol and intramolecular energy $E_{ECEPP/3} = -48.6$ kcal/mol are much higher than the corresponding values for the lowest-energy configuration of Fig. 3b: $E_{TOT} = -277.8$ kcal/mol and $E_{ECEPP/3} = -135.5$ kcal/mol. On the other hand, its solvation energy $E_{SOLV} = -153.0$ kcal/mol is lower than that of Fig. 3b ($E_{SOLV} = -141.3$ kcal/mol) but the differences are smaller than the one in the ECEPP/3 term.

Both kind of configurations appear at the helix-coil transition temperature $T_c = 560(10)$ K. Due to their higher entropy, configurations that resemble the NMR structures are slightly more common for temperatures in the range $520 \text{ K} \leq T \leq 560 \text{ K}$ than the ones that are similar to the crystal structure leading to a positive free energy difference ΔG that is displayed in the inset of Fig. 6. At $T = 520 \text{ K}$, 43(4)% of all configurations are similar to the NMR structures and 40(5)% resemble more the crystal structure. Below $T = 520 \text{ K}$, the intramolecular energy that favors an extended single helix wins over the higher entropy of states with two separate helices. The resulting negative free energy difference ΔG leads to a decrease in the frequency of NMR-like structures, and their contribution is less than 1% at room temperature.

We conjecture that the above relations hold also in nature. The elongated helix of the crystal structure is favored by the intramolecular energies and is the ground state in potential energy. Thermal fluctuations lead to the more flexible configurations with two helices that are observed for the soluted peptide. In a (hydrophobic) membrane environment or when binding to a receptor reduces the entropy of the molecule, PTH(1-34) stays in the 1-helix state that also seems to lead to increase its biological activity¹⁷.

However, the energy function in our simulation overstabilizes the extended α -helix of the PTH(1-34) ground state (the crystal structure). Hence, structures that are found in solution with NMR experiments appear in our simulation with significant frequency only at temperatures more than 200 K above room temperature. Similarly, we find with $T_c = 560(10)$ K a helix-coil transition temperature that is much higher than physiological relevant temperature range. These results clearly point out the limitations of our model. Since our data are consistent with what one would expect in a hydrophobic environment one can conjecture that these limitations of the energy function are mainly due to our solvent approximation. The small variation in the magnitude of the solvent energy in Figs. 1 and

5 (when compared with the ECEPP/3 term) suggests that the OONS term underestimates the protein-solvent interaction. This may be due to the fact that our implicit solvent model does not account for the hydrogen bonds between the polypeptide and water molecules that in water compete with the characteristic intramolecular hydrogen bonding in an α -helix. As a consequence, α -helices are overstabilized, and our energy function rather models the peptide in a hydrophobic environment than in physiological solution. Another problem is that the solvation energy term of Eq. 6 describes actually a free energy and therefore should change with temperature. This effect is neglected in the OONS approximation. Taking such a temperature dependence into account and use of more sophisticated implicit solvent models would likely improve our results. However, we can also not exclude the possibility that the deviation from the NMR results is not due to the solvent term but that our force field, the ECEPP/3 term that describes the intramolecular interactions, biases toward helical conformations.

It follows that other potential energy functions and implicit solvent models have to be chosen for a simulation of PTH(1-34) in solution. However, the failure of our energy function to model correctly the solvated molecule demonstrates also the advantages of our approach. Unlike the earlier simulated annealing simulations of Ref. 21 multicanonical sampling allows one to calculate accurate estimates of the frequency of states and other physical quantities at room temperature. In that way, we have been able to unveil in the present paper the limitations of our energy function. At the same time, our results allow us to understand the behavior of our peptide in a hydrophobic environment (since this is what our energy function models) and to reproduce the crystal structure with high accuracy. Hence, we have shown that multicanonical simulations are not only well-suited for simulations of small peptides but also for numerically more challenging molecules such as the 34-residue peptide PTH(1-34).

IV. CONCLUSION

In summary, we have performed all-atom simulations of PTH(1-34), the biologically active peptide-fragment 1-34 of the human parathyroid hormone. Protein-water interactions are approximated by a solvent-accessible surface term using the OONS parameter set²³. Our results rely on multicanonical sampling and demonstrate that this technique allows one

to overcome the multiple minima problem in simulations of this molecule. Unlike earlier numerical studies²¹ that relied on simulated annealing we find a lowest-energy configurations that has a rmsd of only 0.8 Å to the crystal structure. While previous applications of multicanonical sampling were restricted to small peptides with less than 20 residues, our results (albeit for a molecule with a rather simple structure) establish that the generalized-ensemble approach is also a useful tool for investigation of much larger polypeptides with 30 – 40 residues. Applications to even larger molecules seem to be restricted less by the sampling technique but by the accuracy of the energy function.

Acknowledgments:

Support by a research grant (CHE-9981874) of the National Science Foundation is gratefully acknowledged. Part of the described research was done while I was visiting the John von Neumann Institute for Computing (NIC), located in the FZ Jülich. I like to thank Prof. Grassberger and the institute for kind hospitality and for bearing with my working style.

-
- ¹ P. Ferrara and A. Caffisch, *Proc. Natl. Acad. Sci. USA* **97**, 10780 (2000).
 - ² Y. Duan and P.A. Kollman, *Science* **282**, 740 (1998).
 - ³ Sh. Chowdhury, W. Zhang, Ch. Wu, G. Xiong and Y. Duan, *Biopolymers* **68**, 63 (2003).
 - ⁴ U.H.E. Hansmann and Y. Okamoto, *Curr. Opin. Struc. Biol.* **9**, 177 (1999).
 - ⁵ C.L. Brooks, *Accounts of Chemical Res.*, **35**, 447 (2002).
 - ⁶ A.E. Cardenas and R. Elber, *Proteins: Stru. Fu. Gen.*, **51**, 245 (2003).
 - ⁷ U.H.E. Hansmann, *Chem. Phys. Lett.* **281**, 140 (1997).
 - ⁸ A.E. Garcia and K.Y. Sabonmatsu, *Proteins: Str. Fu. Gen.*, **42**, 345 (2001).
 - ⁹ C.-Y. Lin, C.-K. Hu and U.H.E. Hansmann, *Proteins: Str. Fu. Gen.*, **52**, 436 (2003).
 - ¹⁰ F. Rao and A. Caffisch, *J. Chem. Phys.*, in press.
 - ¹¹ U.H.E. Hansmann and Y. Okamoto, in: D. Stauffer (ed), “Annual Reviews in Computational Physics VI” Singapor: World Scientific (1998), p. 129.
 - ¹² B.A. Berg and T. Neuhaus, *Phys. Lett. B* **267**, 249 (1991).
 - ¹³ U.H.E. Hansmann and Y. Okamoto, *J. Comp. Chem.* **14**, 1333 (1993).
 - ¹⁴ U.H.E. Hansmann and Y. Okamoto, *J. Phys. Chem* **102**, 653 (1998).
 - ¹⁵ N.A. Alves and U.H.E. Hansmann, *J. Chem. Phys.* **117**, 2337 (2002).

- ¹⁶ W. Klaus, T. Dieckmann, V. Wray, D. Schomburg, E. Wingender and H. Mayer, *Biochemistry* **30**, 6936 (1991).
- ¹⁷ L. Jin, S.L. Briggs, S. Chandrasekhar, N.Y. Chirgadze, D.K. Clawson, R.W. Schevitz, D.L. Smiley, A.H. Tashjian, F. Zhang, *J. Biol. Chem.* **275**, 27238 (2000).
- ¹⁸ U.C. Marx, K. Adermann, P. Bayer, W.-G. Forssmann and P. Rösch, *Biochem. Biophys. Res. Comm.* **267**, 213 (2000).
- ¹⁹ J.T. Potts Jr, H.M. Kronenberg, M. Rosenblatt, *Adv. Prot. Chem.* **35**, 323 (1982).
- ²⁰ R. Brommage, C.E. Hotchkiss, C.J. Lees, M.W. Stancill, J.M. Hock and C.P. Jerome, *J. Clin. Endocrinol. Metab.* **84**, 3757 (1999).
- ²¹ Y. Okamoto, T. Kikuchi, T. Nakazawa and H. Kawai, *Int. J. Pep. Prot. Res.* **42**, 300 (1993).
- ²² G. Némethy, K.D. Gibson, K.A. Palmer, C.-N. Yoon, G. Paterlini, A. Zagari, S. Rumsey, H.A. Scheraga, *J. Phys. Chem.* **96**, 6472 (1992).
- ²³ T. Ooi, M. Obatake, G. Némethy, H.A. Scheraga, *Proc. Natl. Acad. Sci. USA* **8**, 3086 (1987).
- ²⁴ F. Eisenmenger, U.H.E. Hansmann, Sh. Hayryan, C.-K. Hu, *Comp. Phys. Comm.* **138**, 192 (2001).
- ²⁵ A.M. Ferrenberg and R.H. Swendsen, *Phys. Rev. Lett.* **61**, 2635 (1988); *Phys. Rev. Lett.* **63**, 1658(E) (1989), and references given in the erratum.
- ²⁶ U.H.E. Hansmann, *Phys. Rev. E.* **56**, 6200 (1997).
- ²⁷ F. Eisenhaber, P. Lijnzaad, P. Argos, C. Sander and M. Scharf, *J. Comp. Chem.* **16**, 273 (1995).
- ²⁸ T. Schaumann, W. Braun and K. Wuthrich, *Biopolymers*, **29**, 679 (1990).
- ²⁹ U.H.E. Hansmann and L. Wille, *Phys. Rev. Lett.* **88**, 068105 (2002).

Figure Captions:

- Fig. 1** Average intramolecular energy $\langle E_{ECEPP/3} \rangle$, solvent energy $\langle E_{SOLV} \rangle$ and total energy $\langle E_{TOT} \rangle = \langle E_{ECEPP/3} + E_{SOLV} \rangle$ of PTH(1-34) as a function of temperature T . The inset displays the specific heat $C(T)$ as a function of temperature T . The data are calculated from a multicanonical simulation of 1,000,000 sweeps using a solvent accessible surface term to approximate protein-water interactions.
- Fig. 2** Average helicity $\langle n_H \rangle$ as a function of temperature T . The inset displays the susceptibility $\chi(T)$ as a function of temperature T . All data points are calculated from a multicanonical simulation of 1,000,000 sweeps using a solvent accessible surface term to approximate protein-water interactions.
- Fig. 3** (a) The crystal structure of PTH(1-34) (PDB code 1ET1); (b) The lowest-energy conformation of PTH(1-34) as determined from a multicanonical simulation with a solvent accessible surface term; (c) Solution structure of PTH(1-34) as determined by NMR (PDB-code 1HPY). (d) One of the configurations resembling the solution structure. Such configurations appear in our simulation with significant frequency only for temperatures closely to but below the helix-coil transition temperature $T_c = 560$ K.
- Fig. 4** Projection of the free-energy landscape (ΔG) of PTH(1-34) at $T = 300$ K on the number of native contacts n_{NC} . The same quantity is plotted for the $T = 560$ K (the critical temperature) in the inset.
- Fig. 5** (a) Free energy difference ΔG_i between configurations with residue i part of an α -helix and such where residue i is not in a helical state. (b) The corresponding total (potential) energy differences ΔE_{TOT} (\square), intramolecular energy differences $\Delta E_{ECEPP/3}$ (\circ) and solvent energy differences $\Delta E_{SOLV}(x)$.
- Fig. 6** Frequency of PTH(1-34) configurations ($1H$) that resemble the crystal structure and frequency of states ($2H$) that are similar to the solution structures of the peptide. The free-energy difference ΔG between both sets of configurations is displayed in the inset. All quantities are shown as function of temperature T . All our data points

are calculated from a multicanonical simulation of 1,000,000 sweeps using a solvent accessible surface term to approximate protein-water interactions.

FIG. 1:

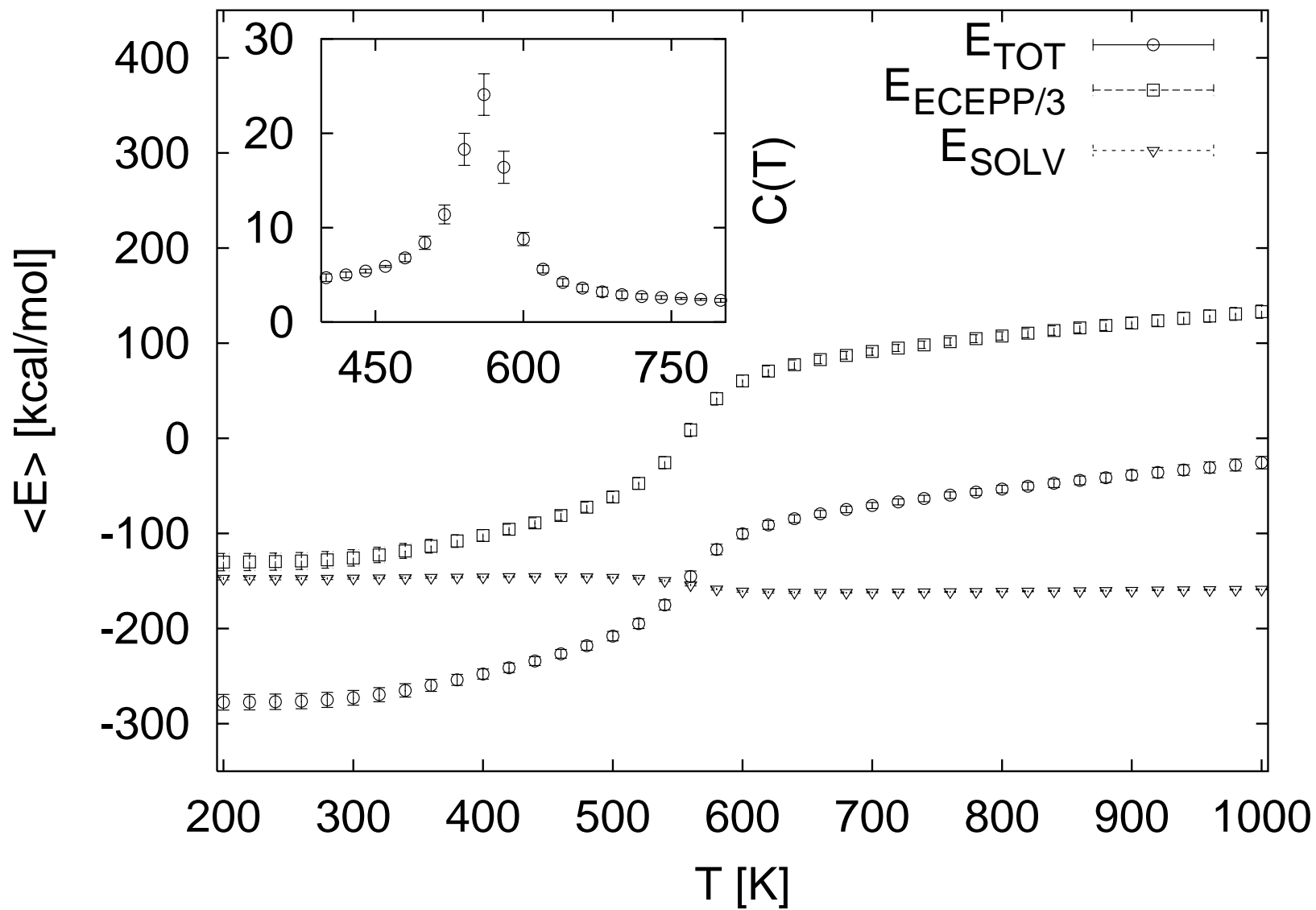
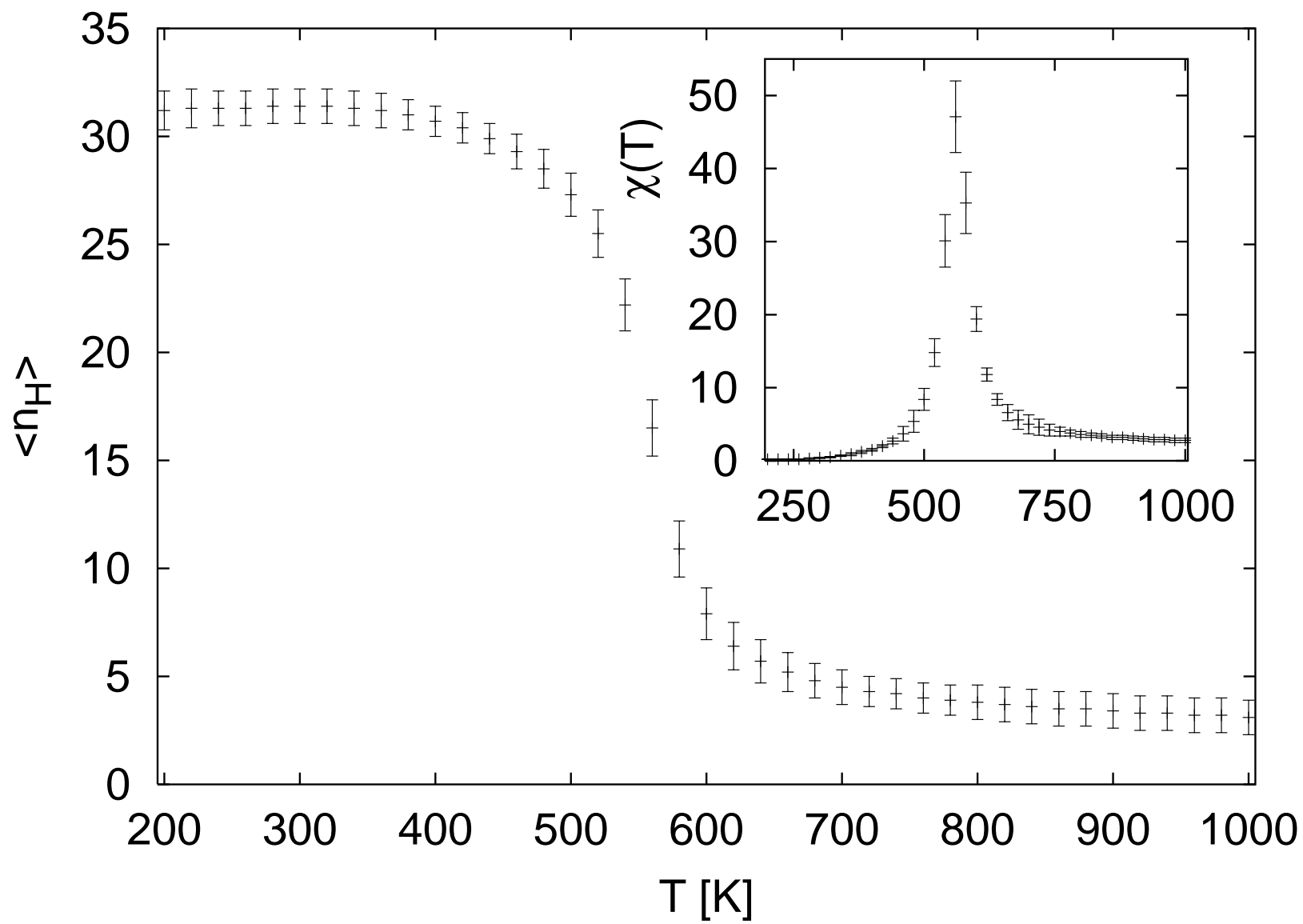


FIG. 2:



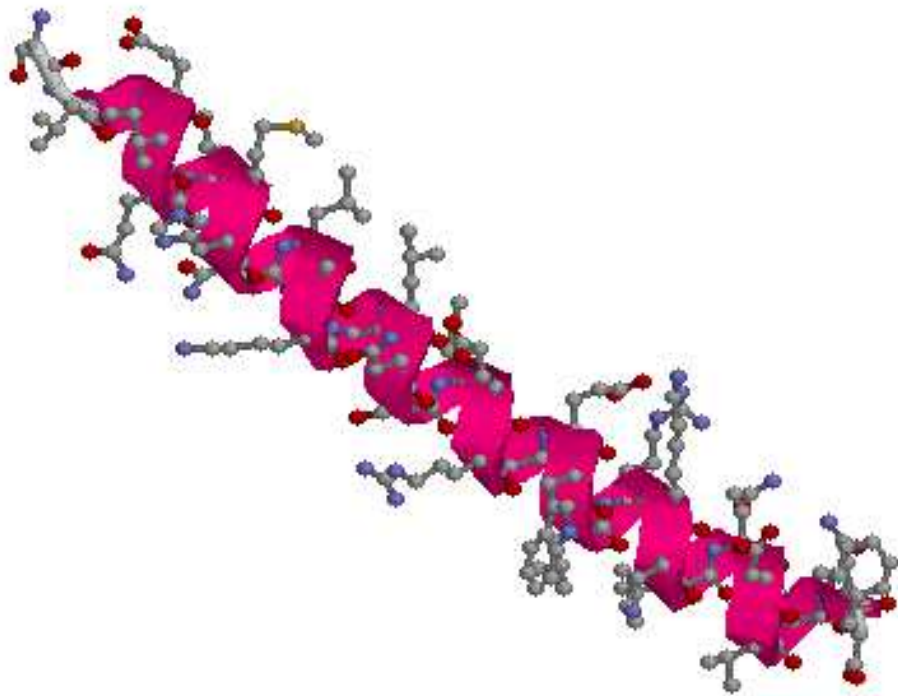


FIG. 3:

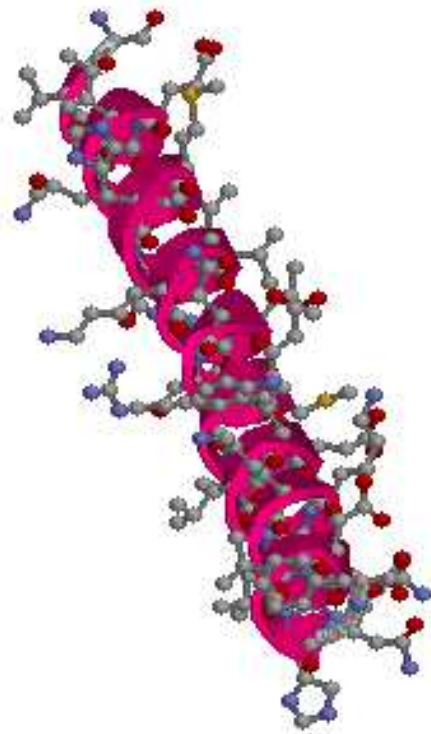


FIG. 4:

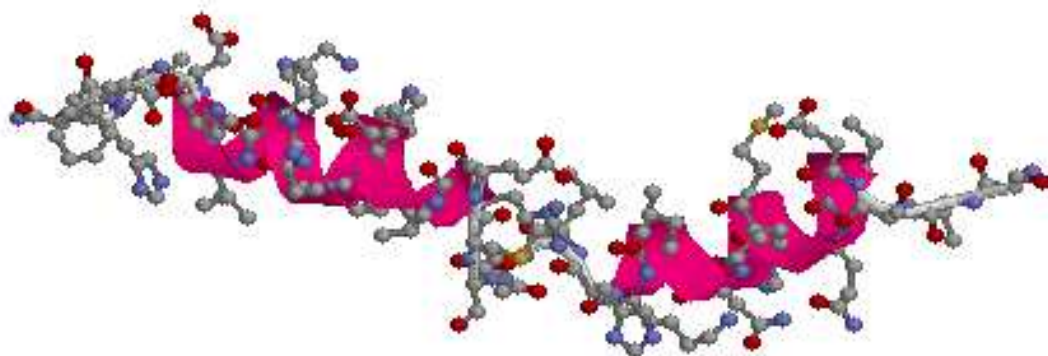


FIG. 5:

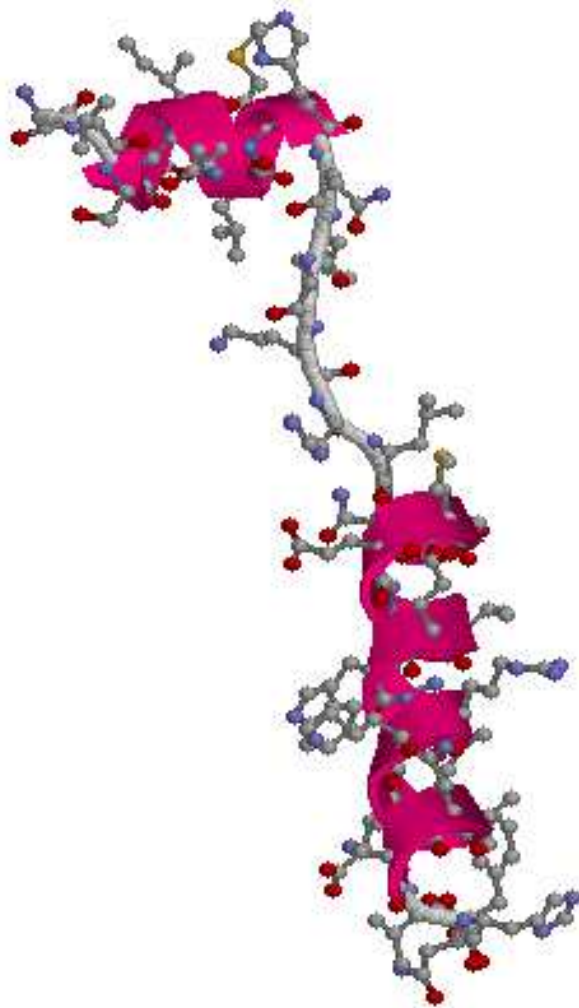
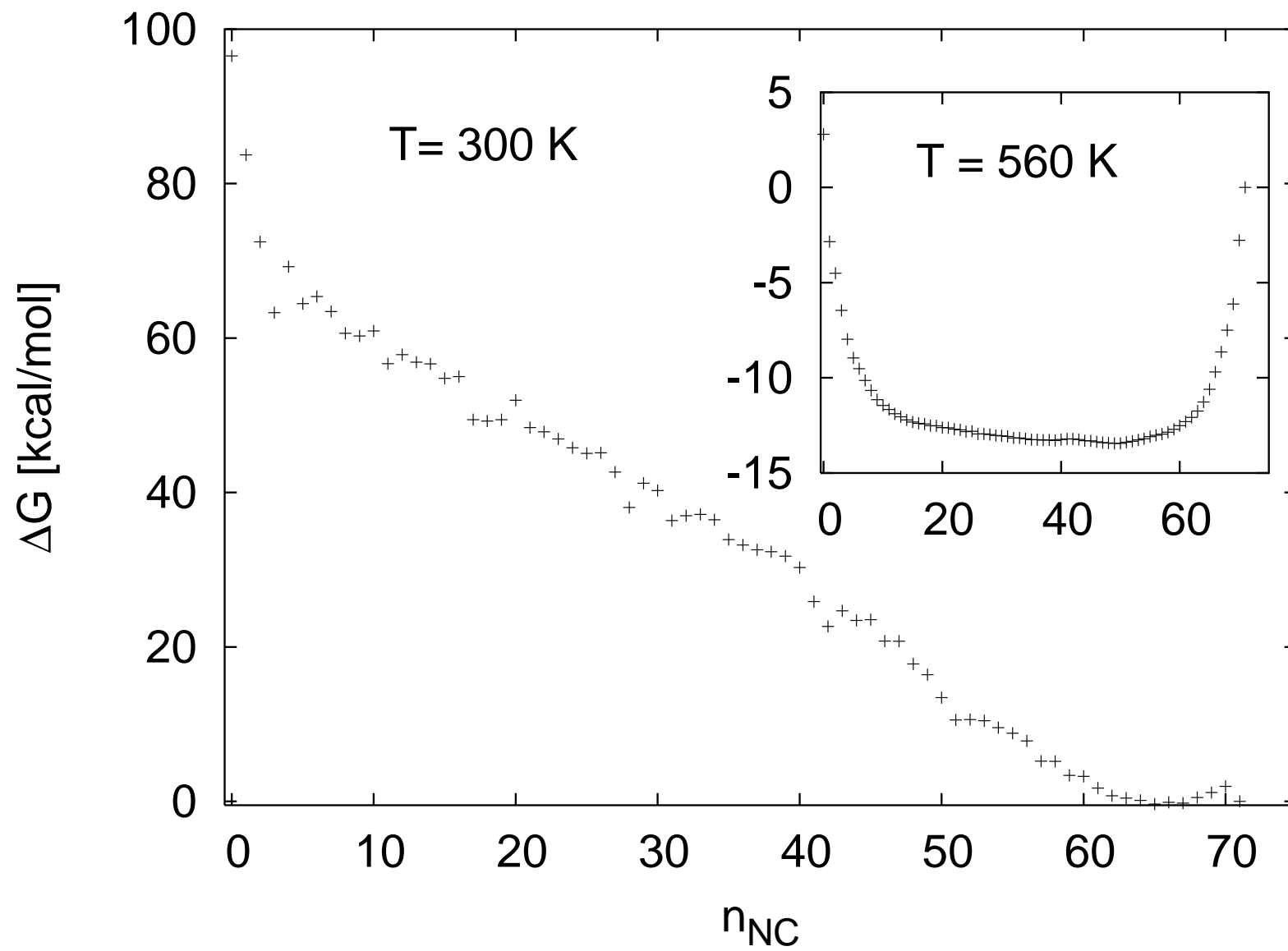


FIG. 6:

FIG. 7:



T = 300 K

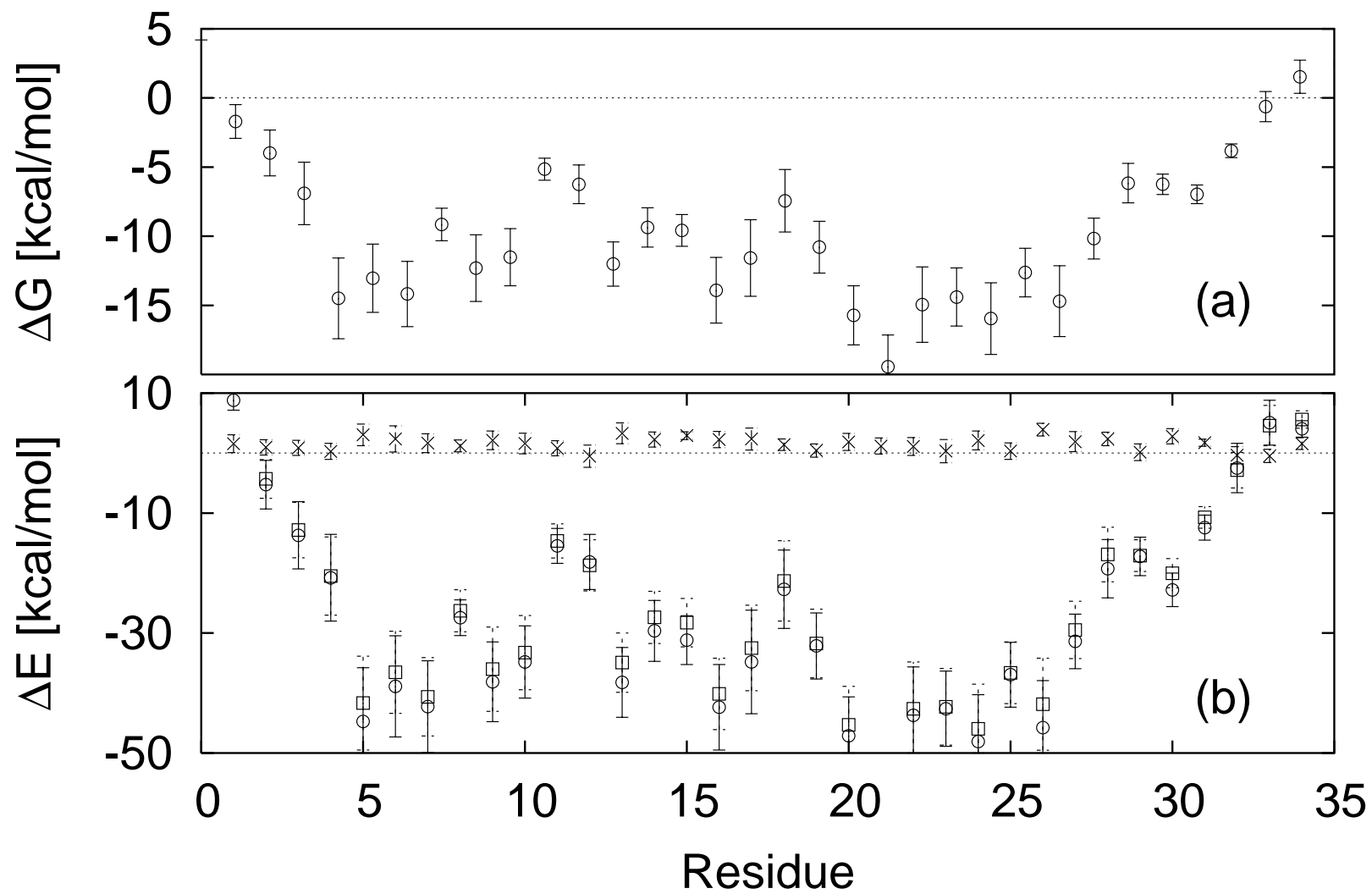


FIG. 8:

FIG. 9:

